Synthesis of Spinel Ferrites in Radiofrequency Thermal Plasma Reactor

J. Szépvölgyi[1,2], L. Gál[1], I. Mohai[1], I. Mészáros[3], J. Gubicza[4]

[1] *Institute of Materials and Environmental Chemistry, Chemical Research Center, Hungarian Academy of Sciences, Budapest, Hungary*
[2] *Research Institute of Chemical and Process Engineering, University of Pannonia, Veszprém, Hungary*
[3] *Research Group for Metals Technology, Budapest University of Technology and Economics, Budapest, Hungary*
[4] *Department of Solid State Physics, Eötvös University, Budapest, Hungary*

Abstract: Formation of nanosized zinc-ferrites and nickel-zinc ferrites from iron- and zinc oxide powders and corresponding nitrate solutions, respectively, was studied in RF thermal plasma conditions. The products were characterized for chemical composition, phase conditions, particle size distribution, morphologies and saturation magnetization. Effects of synthesis conditions on properties of products were studied in details.

Keywords: radiofrequency thermal plasma, spinel, ferrite

1. Introduction

The spinel ferrites of $MeFe_2O_4$ stoichiometry (where Me = Zn^{2+}, Fe^{2+}, Ni^{2+}, Co^{2+}, Cd^{2+}, Mg^{2+}, Mn^{2+} etc.) are widely used as desulfurization agents of flue gases, catalysts [1], materials of electronic- and magnetic data recorder devices [2,3], gas sensors [4], microwave tools [5], magneto-optical equipments [6], drug carriers [7] and materials for cancer treatment [8]. Ferrite devices used in electrical engineering and electronics are generally produced from ferrite powders subjected to forming and sintering at high temperatures.

The ferrite powders are usually produced by one of the following methods:

- heat-treatment of the mixture of metal oxides,
- precipitation of ferrites from solutions and
- sol-gel processing.

Another synthesis route involves thermal decomposition of metal nitrate solutions at high temperatures. First step of the process is the evaporation of solvent followed by the decomposition of nitrates and formation of ferrites [9]. The evaporation, the chemical reaction and the condensation from gas phase take place very rapidly leading to formation of micro- and nanosized particles.

Spinels of $ZnFe_2O_4$ and $Ni_XZn_{(1-X)}Fe_2O_4$ composition constitute a special group of ferrites. They belong to the *Fd3m* crystal group and crystallize in face-centered cubic structure. In normal ferrites, the Zn^{2+} and Ni^{2+} cations are located at tetragonal sites, while the Fe^{3+} cations occupy octagonal ones [10]. The oxygen ions are positioned among the lattice points (Fig. 1).

The magnetic momentum of normal zinc-ferrite spinels is zero. Below the Néel temperature (10K) they are antiferromagnetic, while above it they are paramagnetic. If we provide sufficient energy to a normal ferrite spinel – e.g. by mechanochemical activation [11] or by long-lasting heat treatment – lattice inversion will occur: certain Fe^{3+} cations will be exchanged by Zn^{2+} and Ni^{2+} cations and vice versa. Thus, inverse ferrites with composition of $(Fe^{3+}_Y)[Ni^{2+}_XZn^{2+}_{(1-X)}Fe^{3+}_{2-Y}]O_4$ will be formed. The inverse ferrites are metastable in thermodynamic terms. The smaller the particle size, the easier is the formation of inverse structure. The inverse zinc- and nickel-zinc ferrite spinels are ferrimagnetic materials.

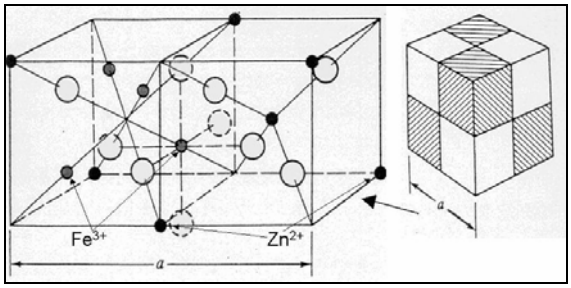

Fig. 1 Crystal structure of zinc ferrites [11]

Thermal decomposition of the corresponding metal salts usually results in formation of normal i.e. paramagnetic zinc- and nickel-zinc ferrites. However, in thermal plasma conditions there is a good chance of inverse spinel formation because in particular systems the reaction temperature is very high, the precursors are heated very rapidly and the products are cooled with a high rate.

In this paper we present the synthesis of normal and inverse spinel ferrites from different precursors in thermal plasma conditions. Special attention was devoted to the correlations among the synthesis conditions and properties of products.

2. Experimental

The experiments were performed in a radiofrequency (RF) thermal plasma reactor operating with a TEKNA PL-35 induction plasma torch at a maximum plate power of 30 kW. Argon was used as plasma gas with a flow rate of 20 $l \cdot min^{-1}$. The sheath gas was a mixture of Ar and O_2 with flow rates of 23 $l \cdot min^{-1}$ and 20 $l \cdot min^{-1}$, respectively.

In this work the following precursors were used for ferrite synthesis:

- mixture of microsized NiO, ZnO and Fe_2O_3 powders with a molar ratio of 1:2,
- ethanol solutions of $Ni(NO_3)_2.6H_2O$, $Zn(NO_3)_2 \cdot 6H_2O$ and $Fe(NO_3)_3 \cdot 9H_2O$ with a salt concentration of 0,65 $mol \cdot dm^{-3}$. The solutions were prepared by the dissolving analytical grade $Ni(NO_3)_2.6H_2O$, $Fe(NO_3)_3 \cdot 9H_2O$ and $Zn(NO_3)_2 \cdot 6H_2O$ powders in technical grade ethanol. The Ni:Zn molar ratios were set to 0.75:0.25, 0.5:0.5 and 0.25:0.75, respectively.

The oxide mixtures were injected into the plasma flame by a PRAXAIR powder feeder, while the nitrate solutions by a TEKNA suspension feeder. The injected precursors were atomized by argon with a flow rate of 3 $l \cdot min^{-1}$ along the centerline of torch or into the tail flame region. In the experiments the following synthesis parameters were varied:

- composition and feed rate of precursors,
- plate power of the RF generator and
- spot of precursor the injection.

The reaction products were mostly collected from the water-cooled reactor wall. Their chemical composition was analyzed by ICP-OES (Thermo Jarrell Ash Atomscan 25). A Philips Xpert XRD apparatus operating with Cu K_α radiation was used to analyze the phase composition. The particle size distribution was measured by laser-diffraction method with a Malvern Mastersizer 2000 system. Morphology of products was studied by SEM (Philips XL30 ESEM) and TEM (Philips CM20). The Ni, Zn and Fe content of individual particles was determined by energy dispersive X-ray fluorescence spectroscopy (EDS; NORAN EDS system).

A specially designed vibrating sample magnetometer (VSM) was applied for measuring the first magnetization curves of reaction products. The VSM is operating on the following principle: if a material is placed into a magnetic field, a dipole moment will be induced which is proportional to its susceptibility and the applied magnetic field. In case of sinusoid vibration, the resulting magnetic flux induces an electrical signal in the detector coils. The induced voltage is proportional to the magnetic moment of the sample, the amplitude and the frequency of vibration. Using a vibration controlled reference coil, the amplitude and frequency dependence can be eliminated and the instrument can be calibrated.

The VSM instrument was designed at the Department of Materials Science and Engineering of BME. In contrast to the traditional Foner-type magnetometers, in this VSM instrument the specimen vibrates along the external magnetic field. Therefore, it is called parallel motion vibrating sample magnetometer (PMVSM). This arrangement has several advantages like increased sensitivity, better signal-to-noise ratio, simpler detector coil arrangement and easier positioning of specimens.

In PMVSM the vibration is driven by a sinusoidal signal with a frequency of 75 Hz. A nickel sphere is used as calibration standard. For the ferrite samples a cylindrical specimen holder was designed.

The initial magnetization curves were measured by magnetizing the samples with an external field of about 5000 A/cm. The complete magnetic saturation could be achieved at about 2000 A/cm. The specimens contained both paramagnetic and ferrimagnetic phases in significant amounts. Contribution of the paramagnetic phase was removed from the magnetization curves. Thus, the actual specific saturation magnetization of ferrimagnetic phase was determined [12].

3. Results and discussion

The experimental conditions and properties of products are summarized in Tables 1 and 2, respectively. The specific energy was defined as energy input related to the feed rate of precursors. In both cases the specific energies are much higher for oxide mixtures than for nitrate solutions. It is explained by the technical characteristics of different feeders and the low solid content of solutions.

Chemical compositions measured by ICP-OES were not listed in Tables 1 and 2 because actually all products had the targeted composition within limits of experimental errors.

It was rather surprising that the d_{50}(l) values of products from nitrate solutions were higher than that of products from solid oxides. The probable reason is the proneness of nanosized particles in the former case for agglomeration. SEM investigations support this assumption (Fig. 2).

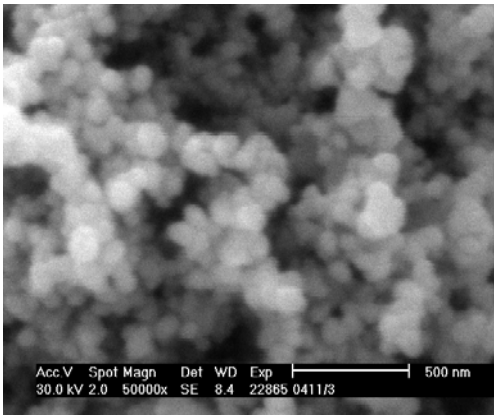

Fig. 2 SEM micrograph of the ZS1 powder

For the zinc ferrite case the saturation magnetization was plotted against the specific energy and the characteristic particle size in Fig. 2. It can be established that the saturation magnetization depends both on the particle size of ferrite powders and the specific energy of powder synthesis, but the effect of specific energy seems to be more pronounced. According to Fig. 3 there is a well defined maximum of saturation magnetization against specific energy in particular synthesis conditions.

Position of the feeding probe determines the thermal history of both precursors and reaction products, and hence, the particle size and saturation magnetization of

ferrite powders. However, in Runs ZP3 and ZP4 with similar feeding positions, zinc ferrites of quite different properties were formed. The high saturation magnetization of ZP3 powder can be attributed to its high magnetite content. On contrary, in the ZP4 powder no magnetite was detected. Its saturation magnetization clearly refers to formation of inverse zinc ferrite.

In the nickel-zinc ferrite case, the saturation magnetization changes against specific energy and characteristic particle size (Fig. 4) in a quite different way as compared to zinc ferrites. In general, higher specific energies result in higher saturation magnetization for both types of precursors. Very low (below 1%) magnetite content was detected in all nickel-zinc ferrite powders. Comparison of saturation magnetization values in Tables 1 and 2 clearly shows the favorable effect of nickel on the magnetic properties of ferrites studied in this work.

Table 1 Synthesis of zinc ferrites

Precursor	$ZnO + Fe_2O_3$				$Zn(NO_3)_2 \cdot 6H_2O + Fe(NO_3)_3 \cdot 9H_2O$					
Run No.	ZP1	ZP2	ZP3	ZP4	ZS1	ZS2	ZS3	ZS4	ZS5	ZS6
Experimental conditions										
Position of feeder probe*	20	20	30	30	10	20	40	60	80	100
Plate power (kW)	25	15	25	15	15	15	15	15	15	15
Precursor feed rate ($g \cdot h^{-1}$)	8	18	22	28	298	289	247	320	265	256
Specific energy ($kWh \cdot g^{-1}$)	3.11	0.87	1.16	0.57	0.05	0.05	0.06	0.05	0.06	0.06
Properties of products										
d_{50}(l) (nm)	78	77	349	72	115	75	163	463	356	369
Magnetite content (m %)	30	21	27	0	7	4	21	15	35	23
Saturation magnetization ($emu \cdot g^{-1}$)	28	30	36	19	7	7	9	10	14	18

* distance from the upper level of induction coil (mm)

Table 2 Synthesis of nickel-zinc ferrites

Precursor	$NiO + ZnO + Fe_2O_3$			$Ni(NO_3)_2 \cdot 6H_2O + Zn(NO_3)_2 \cdot 6H_2O + Fe(NO_3)_3 \cdot 9H_2O$					
Run No.	NZP1	NZP2	NZP3	NZS1	NZS2	NZS3	NZS4	NZS5	NZS6
Experimental conditions									
Position of feeder probe*	20	20	20	20	20	20	80	80	80
Plate power (kW)	25	25	25	15	15	15	25	25	25
Feed rate ($g \cdot h^{-1}$)	6	4	15	327	271	345	97	97	97
Specific energy ($kWh \cdot g^{-1}$)	4.08	5.73	1.66	0.046	0.055	0.044	0.25	0.25	0.25
Properties of products									
d_{50}(l) (nm)	119	63	274	201	243	244	74	182	214
Magnetite content (m %)	< 1								
Saturation magnetization ($emu \cdot g^{-1}$)	35	40	50	34	42	45	38	52	48

* distance from the upper level of induction coil (mm)

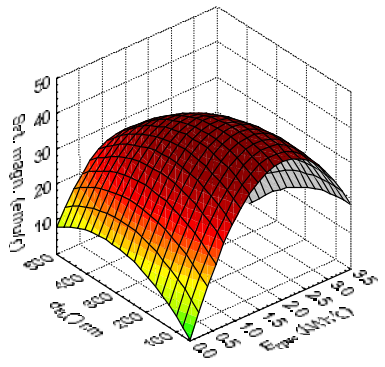

Fig. 3 Saturation magnetization of zinc ferrite powders against specific energy and particle size

The characteristic particle size of nickel-zinc ferrites changes in some extent against the specific energy: higher specific energies led to formation of smaller particles which is explained by the thermal history of the species. However, changes in the feeding position within given limits hardly affected the particle size or the saturation magnetization of nickel-zinc ferrite powders.

The high saturation magnetization values observed for powders from Run Nos. NZP3 and NZS5 make probable formation of inverse spinel structures.

According to EDS measurements (Fig 5), the smaller particles contained a bit more zinc, while the bigger ones a bit more iron as compared to the stoichiometric composition. Grains of nearly stoichiometric composition have d_{50}(l) values of 60 to 80 nm.

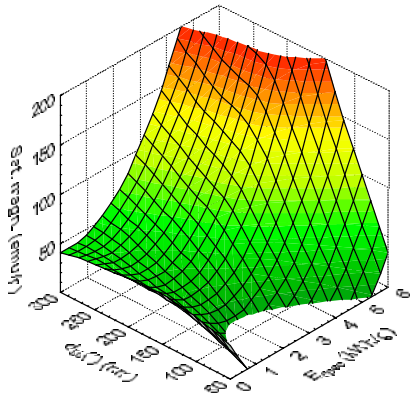

Fig. 4 Saturation magnetization of nickel zinc ferrite powders against specific energy and particle size

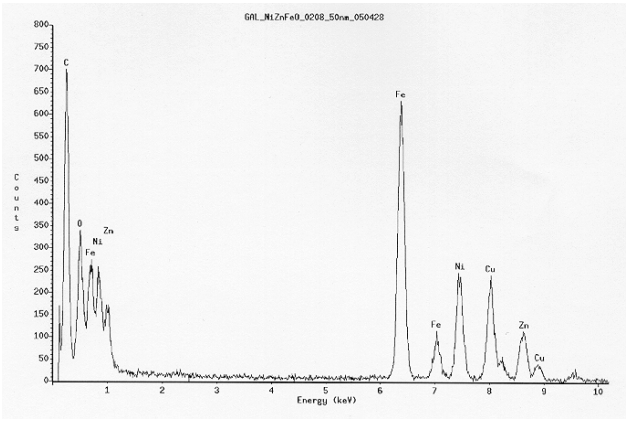

Fig. 5 EDS spectrum of NZP3 powder (d_{50}(l) ~ 50 nm)

4. Conclusions

We proved that in RF thermal plasma conditions nanosized normal and inverse zinc-ferrites and nickel-zinc ferrites could be produced both from oxide powders and ethanol solutions of corresponding nitrates, respectively. The synthesis conditions such as feed rate of precursors and specific energy of processing have an effect both on the morphology and the magnetic properties of ferrite powders. Extent of particular effects, however, depends on the type and feeding position of precursors, as well.

Acknowledgement

This work was supported by the Hungarian Scientific Research (OTKA) Grant No. T047360 and by the GVOP Project No. 3.1.1-2004-05-0031/3.0.

References

[1] Yürüm, Y. (ed): Clean Utilization of Coal: Coal Structure and Reactivity, Cleaning and Environmental Aspects, Kluwer, 1992, NATO ASI Series 370, pp. 221

[2] Sugita N., Maekawa M., Ohta Y.: IEEE Transactions on Magnetics **31**, 2854 (1995).

[3] Oliver, S. A., Yoon, S.D., Kozulin, I.: Applied Physics Letters **76,** 3612 (2000).

[4] Sandu I., Presmanes L., Alphonse P., Tailhades P.: Thin Solid Films **495**, 130 (2006).

[5] Fu Y., Hsu Y. P., Hsu Ch.: Journal of Alloys and Compounds **391,** 185 (2005).

[6] Gut B. X., Zhang H. Y., Zhai H. R.: Physics of Condensed Matters **6,** 1047 (1994).

[7] Rana S., Gallo A., Srivastava R.S., Misra R.D.K.: Acta Biomaterialia **3**(2), 233 (2007).

[8] Pradhan P., Giri J., Banerjee R., Bellare J., Bahadur D.: Journal of Magnetism and Magnetic Materials, **311**(1), 208 (2007).

[9] Economos G.: Journal of the American Ceramic Society, **38**(7), 241 (1955).

[10] Cullity B. D.: Introduction to Magnetic Materials, Addison-Werley, Reading, MA (1972).

[11] Druska P., Steinike U., Sepelák V.: Journal of Solid State Chemistry **146,** 13 (1999).

[12] Mészáros I.: Materials Science Forum **414-4,** 275 (2003).